PROCEEDINGS OF SCIENCE

Study of the Lateral Distribution of EAS Thermal Neutrons Based on ENDA

Fan-Ping Li,[a,*] Hu Liu,[a] Xin-Hua Ma,[b,c] Wei Gao,[b,c,*] Shu-Wang Cui,[d] Tian-Lu Chen,[e,f] Danzengluobu,[e,f] Wen-Chao Gao,[b,g] Xin-Rui Gao,[e,f] Zi-Ao Gong,[d] Hai-Bing Hu,[e,f] Denis Kuleshov,[h] Kirill Kurinov,[h] Bing-Bing Li,[i] Jia-Heng Li,[j] Yang Li,[d] Mao-Yuan Liu,[e,f] Ye Liu,[k] Xi-An Pan,[j] Da-Yu Peng,[e,f] Yao-Hui Qi,[d] Dong Qu,[e,f] Oleg Shchegolev,[h,l] Yuri Stenkin,[h,l] Tian-Shuang Yang,[k] Li-Qiao Yin,[b,c] Heng-Yu Zhang,[e,f] Hui-Qian Zhang,[d] Liang-Wei Zhang[d] and Shi-Yuan Zhang[d]

[a] *School of Physical Science and Technology, Southwest Jiaotong University, Chengdu, Sichuan 610031, China*

[b] *State Key Laboratory of Particle Astrophysics, Institute of High Energy Physics, Chinese Academy of Sciences, Beijing 100049, China*

[c] *TIANFU Cosmic Ray Research Center, Chengdu, Sichuan 610000, China*

[d] *College of Physics, Hebei Normal University, Shijiazhang 050024, China*

[e] *Key Laboratory of Comic Rays, Ministry of Education, Xizang University, Lhasa, xizang 850000, China*

[f] *Science School, Xizang University, Lhasa, Xizang 850000, China*

[g] *University of Chinese Academy of Sciences, Beijing 100049, China*

[h] *Institute for Nuclear Research of the Russian Academy of Sciences, Moscow 117312, Russia*

[i] *College of Physical Science and Technology, Bohai University, Jinzhou, 121013, China*

[j] *School of Physics, Shandong University, Jinan, 250100 China*

[k] *School of Management Science and Engineering, Hebei University of Economics and Business, Shijiazhuang, Hebei 050061, China*

[l] *Moscow Institute of Physics and Technology, 141700 Moscow, Russia*

E-mail: huliu@swjtu.edu.cn, maxh@ihep.ac.cn, liliya@my.swjtu.edu.cn

Hadrons serve as the "skeleton" of Extensive Air Shower (EAS), carrying critical information about cosmic ray composition and energy. Electron-Neutron Detector Array (ENDA) is capable of detecting the electromagnetic components generated by EAS as well as the secondary thermal neutrons produced by hadrons. This report simulates the response of the ENDA detector and conducts an investigation into the lateral distribution of thermal neutrons using simulated data. By selecting various parameters, the fitting performance of different functional models for the thermal neutron's lateral distribution is evaluated. The results indicate that a double exponential function exhibits superior fitting performance for the lateral distribution of thermal neutrons. These findings provide a basis for optimizing the modeling approach for thermal neutron lateral distributions.

39th International Cosmic Ray Conference (ICRC2025)
15–24 July 2025
Geneva, Switzerland

*Speaker

PoS(ICRC2025)265

1. Introduction

When high-energy cosmic ray nuclei enter Earth's atmosphere, they initiate extensive air showers (EAS) through interactions with atmospheric nuclei, generating electromagnetic and hadronic components. Precise measurement of hadronic components provides key insights into cosmic ray composition and energy spectra. When hadronic components interact with ground matter(e.g., soil or building materials), they generate evaporation neutrons. These neutrons gradually lose energy through elastic scattering until reaching thermal equilibrium, defined as thermal neutrons,an effective detection messenger. The Electron-Neutron Detector Array (ENDA),located at 4,400 m altitude on Haizi Mountain (Daocheng, Sichuan, China), comprises 64 detectors organized into four clusters [1]. ENDA simultaneously measures electromagnetic components and thermal neutron signals, providing a unique platform for systematic studies of thermal neutron distribution characteristics.

The lateral distribution of secondary particles in EAS is a crucial quantity in ground cosmic ray observation. This distribution provides the foundation for reconstructing the energy and composition of primary particles. The Nishimura-Kamata-Greisen (NKG) function [2] [3] is typically employed to model the lateral distribution of the electromagnetic component. For hadronic components, the lateral distribution depends significantly on hadron energy, with higher-energy hadrons exhibiting greater concentration near the shower core [4]. Early experiments focused on studying hadronic lateral distributions within 10 meters of the shower core. The Tien Shan experiment reported broad lateral distributions [5]. In the Chacaltaya experiment, high-momentum hadrons were observed at larger distances from the shower axis [6]. Initial parameterizations of hadronic LDFs assumed a power-law form [7]. Later, the Maket-ANI collaboration reported consistency with an exponential form within 5 meters of the core [8]. The KASCADE hadronic calorimeter, with its large detection area and dynamic range, extended hadronic LDF analysis to wider core distances, showing optimal fits using the NKG function [9].

For thermal neutrons produced by hadronic interactions, PRISMA-32 employed a double exponential function for parameterization [10]. This study compares the NKG function and a double exponential function for modeling the lateral distribution of thermal neutrons. Based on Monte Carlo simulations, the double exponential function demonstrated universal superiority. Optimized characteristic parameters of the lateral distribution were extracted, which will be applied to subsequent analyses.

2. Monte Carlo simulation

The EAS development initiated by primary cosmic rays was simulated using CORSIKA (Cosmic Ray Simulations for Kascade) version 77410 [11]. QGSJET-II is utilized for high-energy hadronic interactions, and FLUKA is employed for low-energy hadronic interactions. Two representative primary compositions were considered: proton (A = 1) and iron nuclei(A = 56). The energy of primary particles is fixed at $\log_{10}(E/\mathrm{GeV}) = \{5.5, 5.7, 5.9, 6.1, 6.5\}$, corresponding to the transition region near the cosmic-ray "knee". The zenith angle is fixed at $\theta = \{0°, 28°, 40°, 45°\}$ with full azimuthal coverage ($0° \leq \phi < 360°$). The observation level is set at an altitude of 4400 m above sea level. The shower cores were uniformly distributed within a 15 m radius circle centered on the first cluster of the ENDA.

The response of ENDA to secondary particles was simulated using the Geant4 toolkit [12] with configuration parameters rigorously derived from experimentally measured values: structural parameters of the detector array, material properties of components, and electronics response characteristics.

In this study, the simulation of the detector response covers the entire process from the arrival of Corsika generated secondary particles into the detector to the deposition of energy from the interaction of these particles with the scintillator. The energy deposited by electromagnetic component is converted into number of electrons. For thermal neutron detection, a thermal neutron is considered to be collected if a neutron inelastic interaction occurs in the scintillator that produces ^{7}Li with a deposition energy exceeding 1.4MeV. The experimental principle is detailed in [1], and is not reiterated here. Figure 1 shows the detector response to a primary particle interacting with the ENDA. In the left panel, the electron density recorded by each detector is shown. The right panel displays the neutrons recorded by each detector, with each square indicating the relative positions of the detectors.

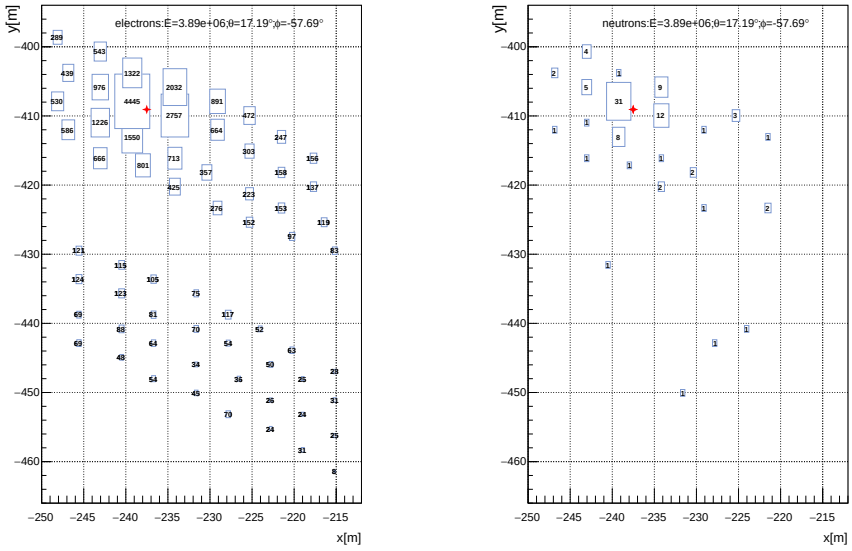

(a) electrons **(b)** thermal neutrons

Figure 1: Layout of ENDA and trigger signal from a single event. (a) electrons; (b) thermal neutrons. The red marker indicates the core position.

3. Lateral distribution of thermal neutron

Thermal neutrons are predominantly produced through the thermalization process of evaporation neutrons generated in hadronic interactions at ground level, the thermal neutron multiplicity exceeds their parent hadrons by up to two orders of magnitude [13]. Figure 2 displays the averaged lateral distributions for proton- and iron-induced showers at fixed energy $\log_{10}(E/\mathrm{GeV}) = 6.1$ and zenith angle $\theta = 0°$. Both primary compositions exhibit a characteristic structure at $R_p \approx 10$ m(R_p

represents perpendicular distance between the neutrons and the shower axis) from the shower core, separating two distinct regimes:

- **Inner region**: A steeply decreasing density profile may dominated by prompt neutron production through hadronic cascade processes near the shower core.
- **Outer region**: A flatter distribution may attributed to the delayed neutrons originating from distant hadrons.

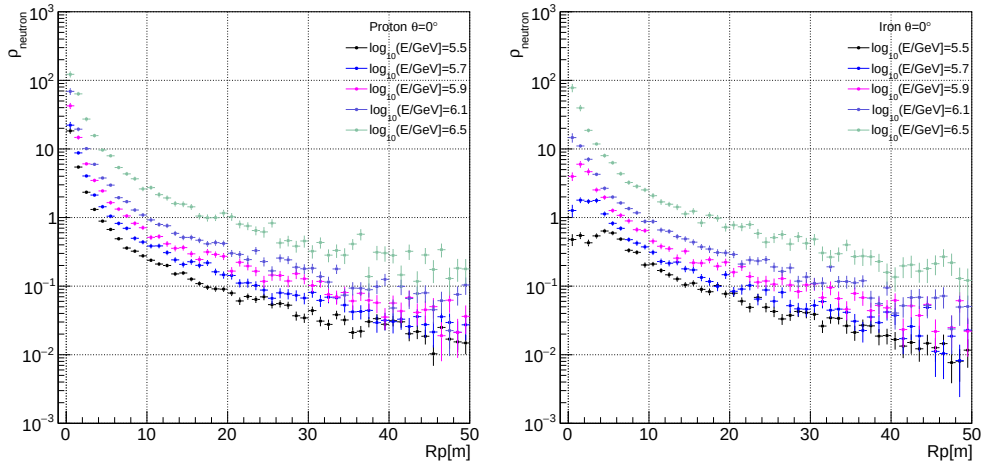

(a) Proton **(b)** Iron

Figure 2: Average lateral distributions of thermal neutrons for proton (left) and iron (right) at $\log_{10}(E/\mathrm{GeV}) = 5.5, 5.7, 5.9, 6.1, 6.5$ with $\theta = 0°$.

The lateral distribution of thermal neutrons differs significantly from electromagnetic components, two parameterization functions were implemented for comparative analysis:

1. NKG function adapted from hadronic component studies in KASCADE [9]:

$$\rho_{NKG}(r, s, N_n) = \frac{N_n}{r_M^2} \frac{\Gamma(4.5-s)}{2\pi\Gamma(s)\Gamma(4.5-2s)} \left(\frac{r}{r_M}\right)^{s-2} \left(1+\frac{r}{r_M}\right)^{s-4.5} \tag{1}$$

with fixed scale radius $R_M = 10$ m and free parameters N_n, s. In equation 1, N_n represents the number of thermal neutrons, s is the age parameter of shower development, r refers to Rp above.

2. Double-exponential function inherited from PRISMA-32 [10]:

$$\rho(r) = A\left(\exp(-\frac{r}{\tau_1}) + B\exp(-\frac{r}{\tau_2})\right) \tag{2}$$

where $\tau_1 = 12.2$, $\tau_2 = 1.77$ are fixed from previous measurements, with A and B as free parameters. Figure 3 compares both functions for vertical showers at $\log_{10}(E/\mathrm{GeV}) = 6.5$, we can find that the double-exponential function can better fit the characteristic structure of the thermal neutron lateral distribution. In order to quantitatively compare the fitting effect of the two functions on the lateral distribution, we chose data with different energies and zenith angles to obtain the χ^2/ndf of the two functions fitting the mean lateral distribution, respectively. As illustrated in Figure 4,

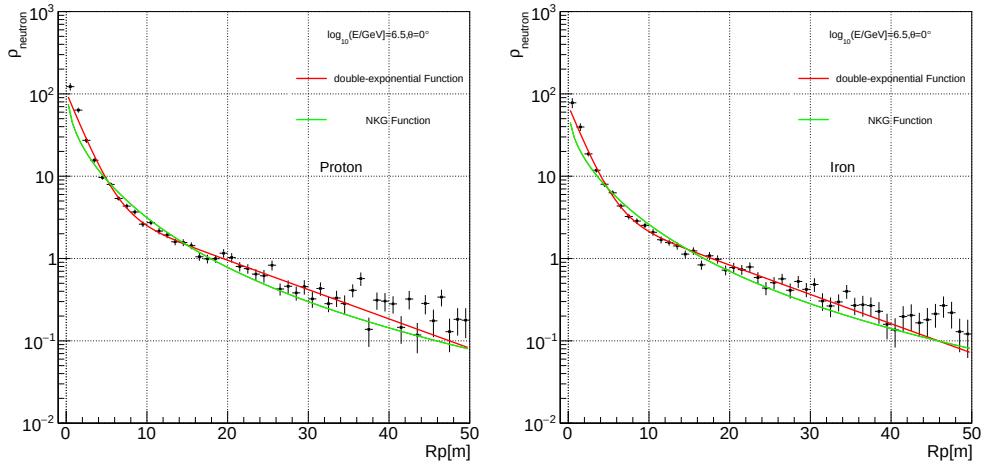

(a) Proton **(b)** Iron

Figure 3: Comparison of fitting functions for proton (a) and iron (b) at $\log_{10}(E/\mathrm{GeV}) = 6.5$ with $\theta = 0°$. The NKG function (green curve) and double-exponential function (green curve) are shown with $R_M = 10$ m and $\tau_1 = 12.2$, $\tau_2 = 1.77$ respectively.

χ^2/ndf fitted by the double-exponential function is relatively smaller and more stable with energy and zenith angle under different simulation conditions. This indicates that it is advantageous to use a double-exponential function to describe the lateral distribution of thermal neutrons.

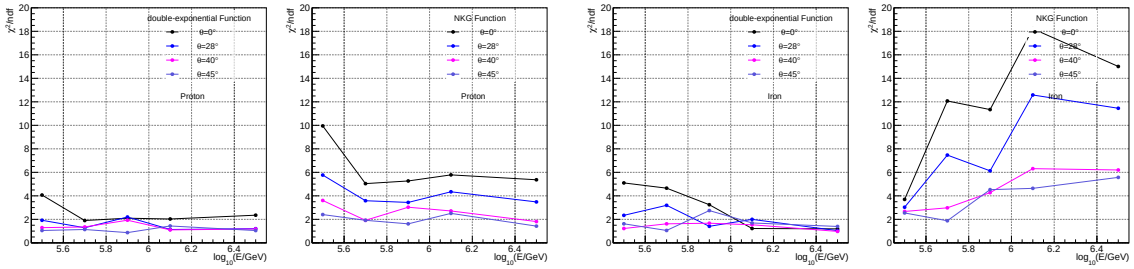

(a) **(b)** **(c)** **(d)**

Figure 4: χ^2/ndf under all simulated energy bins and zenith angles. (a) proton, fitted with double exponential function; (b) proton, fitted with NKG function; (c) iron, fitted with double exponential function; (d) iron, fitted with NKG function.

4. Analysis result

Based on the double-exponential function established in Section 3, we realize the reconstruction of the lateral distribution of thermal neutrons by the maximum likelihood estimation method, where A and B in equation 2 are assumed as free parameters. The fitting results for fixed energies and zenith angles are shown in Figure 5a, where the reconstructed lateral distribution of neutrons has some fluctuations, and the magnitude of the fluctuations is not uniform at different R_p. By

fitting the neutron number density distribution within an R_p bin of the lateral distribution with a Gaussian function, the σ value of the fitting result can be obtained (Figure 5b), and σ is employed to represent the fluctuation of the neutron number density at this R_p. In order to find a parameter

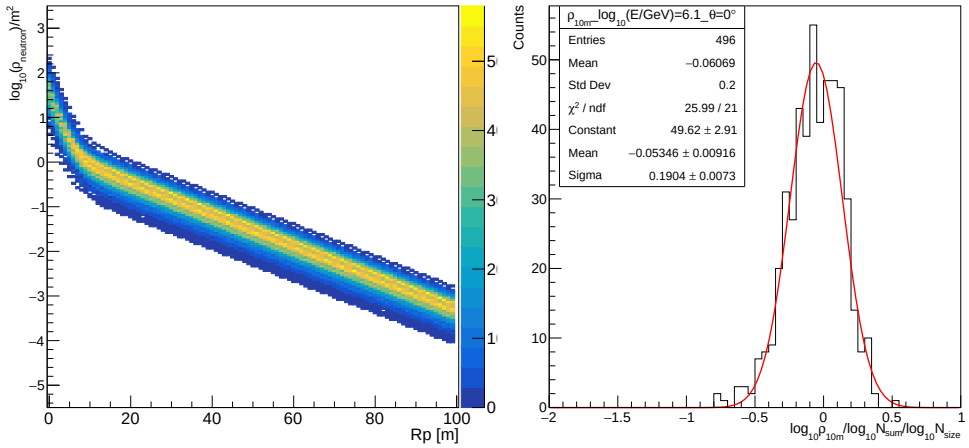

Figure 5: Left panel: Lateral distribution of thermal neutrons at fixed energy and zenith angle; Right panel: Fitting the neutron number density distribution within an R_p bin.

with the smallest fluctuation, Figure 6 shows the variation of σ with R_p for different compositions, energies, and zenith angles, and it can be found that the R_p when σ is the smallest is not fixed, but varies around 10 m. Therefore, we choose the neutron number density at 10 m $\rho_{10\mathrm{m}}$ as a new parameter with a smaller fluctuation.

Current energy reconstruction and composition discrimination of cosmic rays rely on the secondary particle count, which is highly sensitive to the shower core position and exhibits significant fluctuations. In Figure 7, a comparison of the fluctuations of $\rho_{10\mathrm{m}}$ with N_{sum} , N_{size} is shown, where N_{sum} denotes the total number of thermal neutrons recorded by ENDA, and N_{size} denotes the integral over the reconstructed lateral distribution of neutron thermal neutrons. It can be seen that under different conditions, $\rho_{10\mathrm{m}}$ consistently maintains a lower fluctuation compared to N_{sum} and N_{size}, which demonstrates the stability of the parameter $\rho_{10\mathrm{m}}$ under different detection conditions. The advantage of $\rho_{10\mathrm{m}}$ can be presented in more detail in Figure 8, where at energy E=$10^{6.1}$ GeV , zenith angle $\theta = 0°$, the σ of distribution of $\rho_{10\mathrm{m}}$(Proton $\sim$ 19%,Iron $\sim$ 16%) is significantly smaller than one of N_{sum}(Proton $\sim$ 32%,Iron $\sim$ 18%) and N_{size}(Proton $\sim$ 23%,Iron $\sim$ 22%).

5. Summary

This study analyzed the lateral distribution of thermal neutrons in EAS using ENDA. Monte Carlo simulations were conducted to evaluate the performance of the NKG function and a double exponential function in modeling the thermal neutron distribution. Results demonstrated that the double exponential function provides a more accurate fit compared to the NKG function.

A new parameter $\rho_{10\mathrm{m}}$ was obtained by analysing the lateral distribution of thermal neutrons, which exhibited stability under varying energy and zenith angle conditions. These findings suggest that the double exponential function offers a reliable framework for modeling thermal neutron

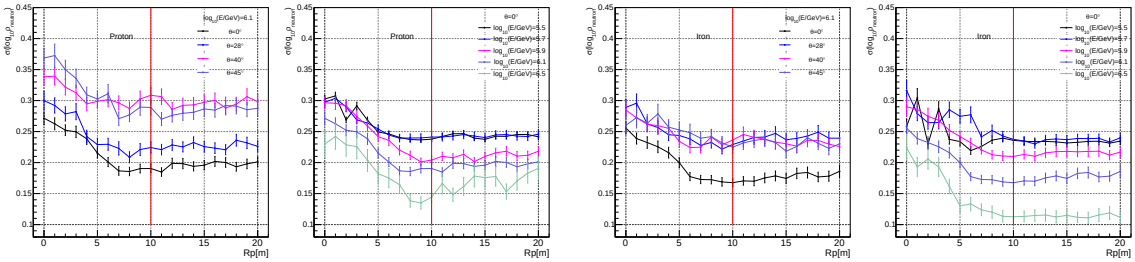

(a) **(b)** **(c)** **(d)**

Figure 6: Distribution of σ at different R_p. (a) Composition:proton,different zenith angle; (b) Composition:proton, different energy; (c) Composition: iron,different zenith angle; (d) Composition:iron,different energy.

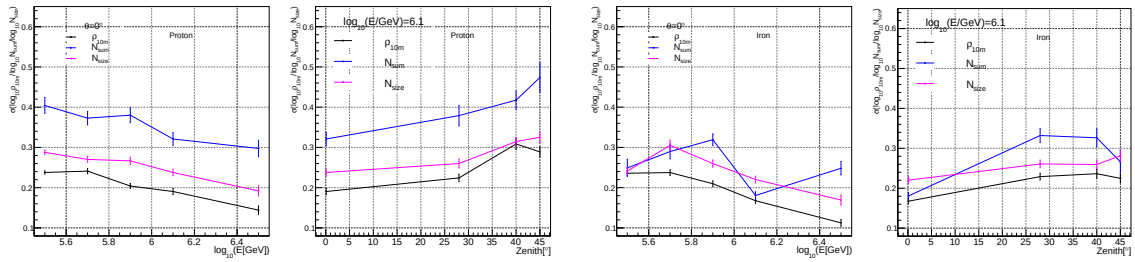

(a) **(b)** **(c)** **(d)**

Figure 7: Resolution parameter σ for different energy bins and zenith angle. (a)(b) Composition:proton; (c)(d) Composition:Iron.

distributions, supporting energy determination and composition separation in cosmic ray energy spectrum studies later.

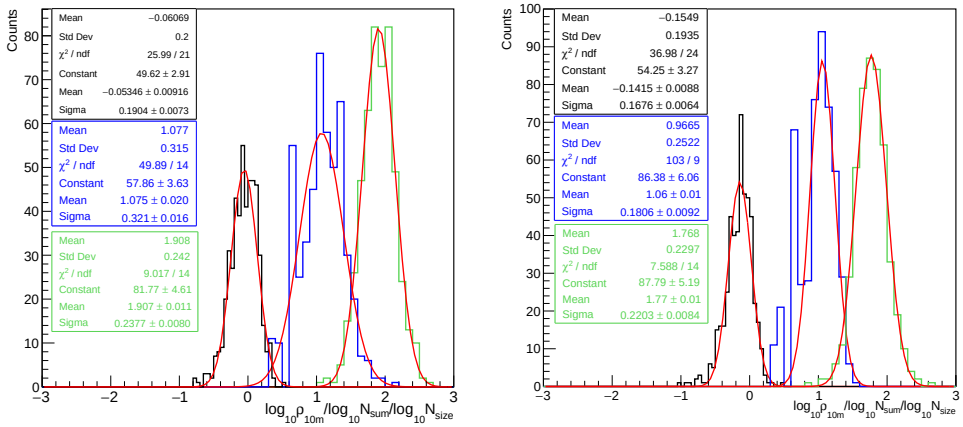

(a) Proton **(b)** Iron

Figure 8: The $\rho_{10\mathrm{m}}$ distribution (black) vs N_{sum} (blue) vs N_{size} (green) for $\log_{10}(E/\mathrm{GeV}) = 6.1$ vertical showers. Red curves show Gaussian fits. Left panel: proton; Right panel: iron.

6. Acknowledgments

This work was supported in China by the National Natural Science Foundation of China (NSFC, No.12205244, 12320101005, No.12263005 and No.12373105) Natural Science Foundation of the Tibet Autonomous Region (grant No.XZ202501ZR0058). The authors would like to thank all staff members who work year-round at the LHAASO site, which is located at an altitude of 4,400 meters above sea level, for maintaining the detectors and ensuring the electricity supply and other components of the experiment run smoothly.

References

[1] Xin-Hua Ma, Yu-Jiang Bi, Zhen Cao, et al. Chapter 1 LHAASO Instruments and Detector technology. *Chinese Physics C*, 46(3):030001, March 2022.

[2] Koichi Kamata and Jun Nishimura. The lateral and the angular structure functions of electron showers. *Progress of Theoretical Physics Supplement*, 6:93–155, 02 1958.

[3] K Greisen. *Progress in Cosmic Ray Physics Vol. III*, 1956.

[4] K. Greisen. Cosmic Ray Showers. *Annual Review of Nuclear Science*, 10(1):63–108, 1960.

[5] T. V. Danilova et al. Proc. *19th ICRC*, 7:40, 1985.

[6] H. Hasegawa et al. High energy nuclear active particles in extensive air showers at 5200 m altitude. *9th ICRC*, 2:645, 1965.

[7] Giuseppe Cocconi. *Extensive Air Showers*, pages 215–271. Springer Berlin Heidelberg, Berlin, Heidelberg, 1961.

[8] S. V Ter-Antonian et al. Energy spectrum and hadron lateral distribution in eas at mountain altitude. maket-ani experiment. *ICRC*, 1:369, 1995.

[9] T Antoni, W.D Apel, et al. Electron, muon, and hadron lateral distributions measured in air showers by the kascade experiment. *Astroparticle Physics*, 14(4):245–260, 2001.

[10] Yuri Stenkin, D. Gromushkin, Petrukhin, et al. EAS thermal neutron lateral and temporal distributions. *ICRC*, 12 2015.

[11] D. Heck, J. Knapp, J. N. Capdevielle, G. Schatz, and T. Thouw. *CORSIKA: a Monte Carlo code to simulate extensive air showers.* 1998.

[12] Allison et al. Geant4 developments and applications. *IEEE Transactions on Nuclear Science*, 53(1):270–278, 2006.

[13] Yuri Stenkin, Victor Alekseenko, Gromushkin, et al. Thermal neutron flux produced by EAS at various altitudes. *Chinese Physics C*, 37, 04 2012.